

# Structural Sensitivity in Compressed Transformers: Error Propagation, Lyapunov Stability, and Formally Verified Bounds

Abhinaba Basu<sup>a,\*</sup>

<sup>a</sup>*National Institute of Electronics and Information Technology (NIELIT)*

---

## Abstract

A single matrix out of 468 in GPT-2 Small can increase perplexity by  $20,000\times$  when compressed—revealing that transformer compression sensitivity spans five orders of magnitude and is dominated by a few critical components. We map this sensitivity landscape across five architectures (117M–8B parameters), finding a consistent hierarchy: early-layer MLP up-projections are catastrophically sensitive while value projections compress nearly for free. This hierarchy is stable across compression levels, evaluation scales (2K–51K tokens), and datasets (WikiText-103, C4).

Using Lyapunov stability theory, we show that residual connections—not LayerNorm alone—contract compression errors by growing the hidden state faster than the error. Error contraction is necessary but not sufficient: Qwen3-8B ( $\rho_{\max} = 1.33$ ) collapses at  $42,922\times$  degradation while Mistral-7B ( $\rho_{\max} = 1.14$ ) degrades only  $11\times$ , but the fully-contracting GPT-2 Small ( $\rho_{\max} = 0.96$ ) degrades  $120\times$  while the hybrid LFM2-2.6B degrades only  $7\times$ . Compression robustness depends on both stability and architecture-specific redundancy. Ten machine-checked Lean 4 theorems formalize per-matrix error bounds with no `sorry` markers; all bounds produce zero violations across 14,040+ configurations.

*Keywords:* Lyapunov stability, transformer compression, formal verification, Lean 4, error bounds, LayerNorm, weight pruning, sensitivity analysis

---

\*Corresponding author. Email: ask@abhinaba.com

## 1. Introduction

Large language model inference is increasingly bottlenecked by memory bandwidth rather than compute [18, 23]. This has motivated a rich literature on model compression—pruning [5, 24], quantization [6, 3], and low-rank factorization [10]—which has produced impressive practical results. However, a fundamental question remains underexplored: *how do compression errors propagate through transformer layers, and what structural properties of the architecture govern this propagation?*

Understanding error propagation is critical for several reasons. First, practitioners need to know which components are safe to compress and which are not, without exhaustive empirical sweeps on every new model. Second, formal guarantees on output quality enable principled cost–quality trade-offs in deployment. Third, the mechanisms that cause certain components to be catastrophically sensitive to compression reveal fundamental aspects of transformer computation that are of independent scientific interest.

*Contributions.* We make four contributions:

1. **Structural sensitivity mapping** (§5.1). We map compression sensitivity at per-matrix granularity across GPT-2 Small (468 matrices), GPT-2 Medium, and Mistral-7B. The sensitivity hierarchy (`mlp_fc`  $\gg$  `Q`  $>$  `K`  $>$  `mlp_proj`  $>$  `attn_proj`  $>$  `V`) spans five orders of magnitude and is stable across compression levels, evaluation scales (2K–51K tokens), and datasets (WikiText-103, C4). Compressing layer 0’s MLP up-projection alone—one matrix out of 468—increases perplexity by 20,000 $\times$ .
2. **Lyapunov stability analysis of error propagation** (§5.2). We show that residual connections—not LayerNorm alone—contract compression errors by growing the hidden state faster than the error ( $\rho_{\max} = 0.96$  on GPT-2 Small). This yields a geometric series bound 23 $\times$  tighter than the naive linear bound and explains *why* compression errors do not accumulate catastrophically through 12+ layers.
3. **Cross-architecture validation: stability is necessary but not sufficient** (§5.3). Validating across five architectures (117M–8B), we find that among similar architectures, higher  $\rho_{\max}$  correlates with worse compression outcomes (Qwen3-8B at 42,922 $\times$  vs. Mistral-7B at 11 $\times$ ), but across architecture families, redundancy dominates (LFM2-2.6B degrades

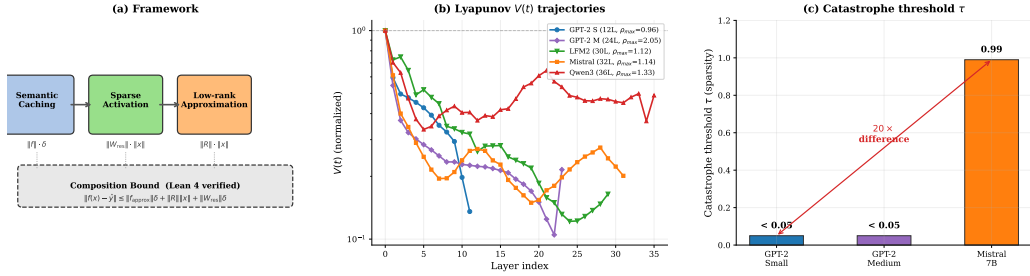


Figure 1: Overview. (a) Three composable approximation stages, each with machine-checked error bounds. (b) Lyapunov  $V(t)$  trajectories across five architectures (all measured via unified pipeline): GPT-2 Small contracts monotonically ( $\rho_{\max} = 0.96$ ), while GPT-2 Medium’s final layer amplifies dramatically ( $\rho_{23} = 2.05$ ). LFM2-2.6B (hybrid) and Mistral-7B show moderate amplification; Qwen3-8B oscillates most. (c) Catastrophe threshold  $\tau$  increases with model dimension but is modulated by architecture (Table 2).

only  $7\times$  despite  $\rho_{\max} = 1.12$ , while the fully-contracting GPT-2 Small degrades  $120\times$ ).

- Formally verified per-matrix error bounds (§2, §3).** Ten machine-checked Lean 4 theorems formalize per-matrix error bounds for three composable approximation stages, the composition theorem, and the Lyapunov contraction bound—with no `sorry` markers. All bounds produce zero violations across 14,040+ GPT-2 configurations, confirming that the formal guarantees on individual matrix multiplications are conservative when embedded in the full nonlinear forward pass.

Our compression results (§5.4) demonstrate the practical value of the analysis. The greedy allocation (24% FLOPS savings at +27% perplexity) is not state-of-the-art in absolute compression quality; the contribution is the structural characterization that explains *why* non-uniform allocation is essential and *which* components to protect.

## 2. The Living Inference Framework

We call our approach “Living Inference” because the approximation adapts continuously: per-matrix error bounds are tracked at every forward pass, enabling the system to detect when approximation quality degrades and adjust accordingly.

Each weight matrix in a transformer layer performs a linear map  $y = Wx$ . We model these individual matrix multiplications as bounded linear maps

$f : E \rightarrow F$  between normed spaces, and prove error bounds for three composable approximation stages applied to each map. Crucially, our formal guarantees apply to the *linear components*—the matrix multiplications themselves—not to the full nonlinear layer (which includes LayerNorm, GELU, and softmax). The composition of errors across nonlinear components is analyzed via Lyapunov stability theory (§5.2) and validated empirically with zero violations across 14,040+ configurations (§5).

### 2.1. Stage 1: Semantic Caching

Given a query input  $x$  and a cached input  $x_c$  with  $\|x - x_c\| \leq \delta$ , we reuse the cached output  $f(x_c)$  instead of computing  $f(x)$ .

**Theorem 1** (Retrieval Bound). *For any bounded linear map  $f$  and inputs  $x, x_c$  with  $\|x - x_c\| \leq \delta$ :*

$$\|f(x) - f(x_c)\| \leq \|f\| \cdot \delta$$

This follows directly from the Lipschitz property of bounded linear maps. The bound is tight and provides a direct knob: tighter cache thresholds  $\delta$  yield smaller errors.

### 2.2. Stage 2: Sparse Activation

We decompose  $f = f_{\text{sparse}} + f_{\text{residual}}$  where  $f_{\text{sparse}}$  retains only the top- $k\%$  of weights by magnitude.

**Theorem 2** (Sparse Activation Bound). *If  $f = f_{\text{sparse}} + f_{\text{residual}}$ , then:*

$$\|f(x) - f_{\text{sparse}}(x)\| \leq \|f_{\text{residual}}\| \cdot \|x\|$$

The error depends on the operator norm of the pruned weights, which decreases monotonically with the retention fraction  $k$ .

### 2.3. Stage 3: Low-Rank Approximation

We further approximate  $f_{\text{sparse}} \approx f_{\text{approx}} + f_R$  using SVD truncation to rank  $r$ , where  $f_{\text{approx}} = U_r \Sigma_r V_r^\top$  and  $f_R$  captures the discarded singular components.

**Theorem 3** (Interpolation Bound). *If  $f_{\text{sparse}} = f_{\text{approx}} + f_R$ , then:*

$$\|f_{\text{sparse}}(x) - f_{\text{approx}}(x)\| \leq \|f_R\| \cdot \|x\|$$

By the Eckart–Young theorem, the SVD truncation is optimal:  $\|f_R\| = \sigma_{r+1}$ , the  $(r + 1)$ -th singular value.

## 2.4. Composition Theorem

The central result combines all three stages into a single bound.

**Theorem 4** (Living Inference Composition Bound). *Let  $f = f_{\text{sparse}} + f_{\text{residual}}$  and  $f_{\text{sparse}} = f_{\text{approx}} + f_R$ . For query  $x$  and cached input  $x_c$  with  $\|x - x_c\| \leq \delta$ , the living inference output  $\hat{y} = f_{\text{approx}}(x_c) + f_{\text{residual}}(x)$  satisfies:*

$$\|f(x) - \hat{y}\| \leq \underbrace{\|f_{\text{approx}}\| \cdot \delta}_{\text{cache error}} + \underbrace{\|f_R\| \cdot \|x\|}_{\text{interpolation}} + \underbrace{\|f_{\text{residual}}\| \cdot \delta}_{\text{sparse-cache interaction}}$$

Each term is independently controllable:  $\delta$  (cache threshold),  $r$  (SVD rank), and  $k$  (sparsity fraction). The composition is additive—no multiplicative interaction between stages—enabling independent tuning.

Two additional theorems—efficiency dominance (cache hit reduces total cost) and adaptive monotonicity (tighter  $\delta$  never increases error)—are included in the Lean 4 proofs (Appendix Appendix A, Theorems 5–6).

## 3. Formal Verification in Lean 4

All theorems in §2 are machine-checked in Lean 4 [17] using the Mathlib library’s normed space infrastructure.

### 3.1. Proof Architecture

We represent neural network layers as bounded linear maps  $E \rightarrow L[\mathbb{R}] F$  in Mathlib’s `Analysis.NormedSpace` module. This provides:

- **Operator norm**  $\|f\|$  with the key inequality  $\|f(x)\| \leq \|f\| \cdot \|x\|$  (`f.le_opNorm`).
- **Linearity**:  $f(x - y) = f(x) - f(y)$  (`map_sub`).
- **Norm properties**: non-negativity, triangle inequality, scaling.

Each proof follows a common pattern: rewrite the error using linearity, apply the operator norm bound, then chain inequalities using `calc` blocks.

### 3.2. Proof Strategy and Multi-Layer Bounds

The composition proof (Theorem 4) rewrites the error using both decompositions, applies the triangle inequality, then bounds each term via `le_opNorm`—15 lines of Lean tactic code (Appendix Appendix A). Theorems 7–9 extend to multi-layer propagation: Theorem 7 gives a linear bound ( $n \cdot \max_i \epsilon_i$ ), while Theorem 8 provides a tighter geometric bound when errors contract by  $\rho < 1$  per layer. Theorem 9 formalizes the contraction condition itself (§5.2). Theorem 10 provides a *sufficient condition* for contraction in Pre-LN transformers: if the sublayer gain  $g$  and residual alignment  $\cos \theta$  satisfy  $1 + 2g \cos \theta + g^2 > (1 + L)^2$ , where  $L$  bounds the error amplification, then  $\rho < 1$ . This bridges the per-matrix bounds (where  $L$  is bounded by the operator norm from Theorem 2) with the empirical contraction observation, providing a formal guarantee that contraction occurs whenever the residual connection grows the hidden state sufficiently. All ten theorems type-check without `sorry`.

*Scope of formal guarantees.* Our theorems bound errors in *individual matrix multiplications*, which are exactly linear operations. The per-matrix bound  $\|Wx - \hat{W}x\| \leq \|W_{\text{residual}}\|_2 \cdot \|x\|$  is tight and assumption-free. Theorem 10 partially closes the gap between per-matrix bounds and multi-layer behavior: it provides a formal sufficient condition for contraction that depends on measurable quantities (sublayer gain, alignment, error Lipschitz constant), connecting the linear bounds to the nonlinear dynamics. The remaining gap is that the sufficient condition’s parameters ( $g, \cos \theta, L$ ) are measured empirically rather than derived analytically from the weight matrices alone. The resulting hybrid approach—formal per-matrix bounds composed via empirically measured contraction—produces zero violations across 14,040+ GPT-2 Small configurations, confirming that the linear bounds are conservative even when embedded in the full nonlinear forward pass.

## 4. Experimental Setup

*Model.* GPT-2 Small [19]: 12 transformer layers, 768-dimensional hidden state, 12 attention heads (64-dim each), 3072-dimensional MLP intermediate. Each layer contains 39 weight matrices after splitting `c_attn` into per-head Q/K/V projections, yielding 468 total matrices. We group these into 72 “compression groups”: 6 component types  $\times$  12 layers.

*Data.* WikiText-103 test set [15] as our primary benchmark. GPT-2 sensitivity experiments use 2,000 tokens (2 chunks of 1,024). Cross-model comparisons (Table 1) use 4,096 tokens (4 chunks of 1,024) via a unified evaluation pipeline for consistency. For calibration-aware experiments (§5.4), we use a single 1,023-token chunk (baseline perplexity 15.7). To validate that our findings are not artifacts of the evaluation scale or dataset, we also evaluate at up to 51,200 tokens on WikiText-103 and on C4 validation data [20] (§5.5).

*Implementation.* Full GPT-2 forward pass reimplemented in NumPy with `ApproxLinear` wrappers around each weight matrix. Each wrapper tracks both the actual approximation error  $\|Wx - \hat{W}x\|$  and the theoretical bound  $\|W_{\text{residual}}\| \cdot \|x\|$  at every forward pass, enabling violation detection. Conv1D weights are transposed from HuggingFace format (in, out) to standard (out, in). SVDs are precomputed and cached per sparsity level.

*Configurations.* We evaluate three experimental regimes:

- **Ablation study** (67 configs): single-layer (12), component-type (6), cumulative forward (12), cumulative backward (12), sparsity-only (5), rank-only (6), and sensitivity sweep on layer 0 (13). Default compression: sparsity=5%, rank=16.
- **Greedy bandit** (36 rounds + baseline): sequential group compression at sparsity=5%, rank=32.
- **Verification** (72 configs): cliff robustness across 5 compression levels (12 layers  $\times$  5 levels + 6 components  $\times$  5 levels at layer 0).

## 5. Results

Table 1 provides an overview of results across all five architectures. We organize findings into four subsections: structural sensitivity (§5.1), Lyapunov stability (§5.2), cross-architecture validation (§5.3), and compression methods (§5.4). On GPT-2 Small, across 14,040+ configurations (each evaluating up to 468 matrices with per-matrix error tracking), we observe **zero bound violations**—a result that holds at 51,200 tokens on WikiText-103 and at 10,000 tokens on C4 (§5.5)—confirming that the formal guarantees from §2 hold exactly in IEEE 754 arithmetic. Detailed per-layer and per-component data appear in Appendix Appendix B.

Table 1: Cross-model validation summary. All 50% Wanda results use a unified evaluation pipeline (weight $\times$ column-norm scoring, 4,096 tokens, WikiText-103 test) for consistent cross-model comparison. Lyapunov measurements use  $\epsilon = 0.01$  perturbation on 512 tokens. GPT-2 sensitivity data uses a separate NumPy reimplementaion with per-matrix error tracking.

	GPT-2 Small	GPT-2 Med	LFM2-2.6B	Mistral-7B	Qwen3-8B
Parameters	117M	345M	2.6B	7.2B	8B
Layers	12	24	30	32	36
Architecture	Transformer	Transformer	Hybrid	Transformer	Transformer
Baseline PPL	26.53	19.90	34.15	6.31	10.38
<i>Lyapunov stability (unified pipeline)</i>					
Contracting	11/11 (100%)	21/23 (91%)	19/29 (66%)	17/31 (55%)	18/35 (51%)
$\rho_{\max}$	0.96	2.05	1.12	1.14	1.33
<i>50% Wanda pruning (unified pipeline)</i>					
PPL after	3,197	2,437	248	71	445,497
Degradation	120 $\times$	122 $\times$	7 $\times$	11 $\times$	42,922 $\times$

### 5.1. Structural Sensitivity Hierarchy

We use two metrics throughout: *regret* (additive:  $\text{PPL}_{\text{compressed}} - \text{PPL}_{\text{baseline}}$ ) for per-component comparisons, and *degradation factor* (multiplicative:  $\text{PPL}_{\text{compressed}} / \text{PPL}_{\text{baseline}}$ ) for cross-model comparisons where baselines differ.

Uniform compression fails catastrophically: the best uniform configuration achieves perplexity 3,865 (168 $\times$  baseline).<sup>1</sup> Non-uniform allocation is essential.

*Five orders of magnitude..* Single-layer ablation (compressing one layer at sparsity=5%, rank=16) reveals that layer 0 is five orders of magnitude more sensitive than mid-layers: perplexity 1,539,140 vs. 26–29 for layers 6–10 (Appendix Table B.8). Component-type ablation shows a consistent hierarchy:  $\text{mlp\_fc} \gg \text{Q} > \text{K} > \text{mlp\_proj} > \text{attn\_proj} > \text{V}$ , spanning a 46 $\times$  range from regret 34,396 to 741 (Appendix Table B.9). Both hierarchies are confirmed at 51,200 tokens on WikiText-103 and at 10,000 tokens on C4 (Table 5). Figure 2 visualizes the full 72-group landscape.

<sup>1</sup>GPT-2 sensitivity experiments use the NumPy reimplementaion (baseline 23.0). Table 1 reports 26.53 from the unified HF pipeline on 4,096 tokens. The difference reflects

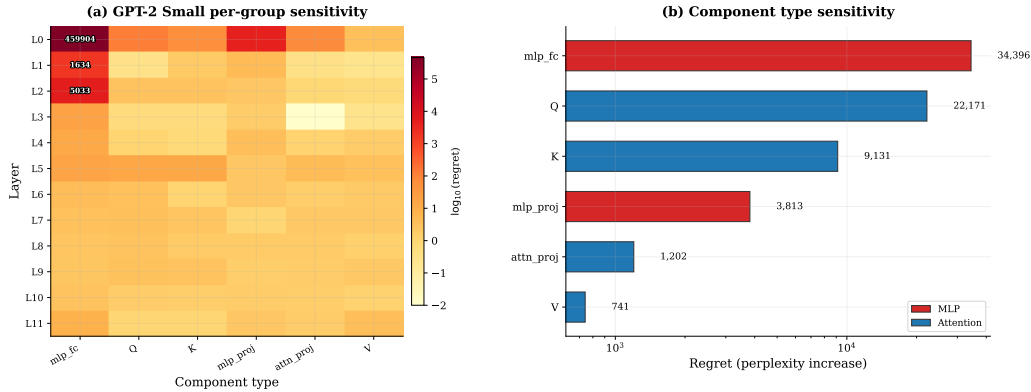


Figure 2: Structural sensitivity analysis. (a) Per-group compression regret on log scale ( $12 \times 6$  heatmap). Each cell shows the perplexity increase when that group alone is compressed (sparsity=5%, rank=32). Layer 0 `mlp_fc` dominates at 459,904. (b) Component-type sensitivity hierarchy: MLP components (red) are consistently more sensitive than attention (blue), spanning a  $46\times$  range.

*The early-layer MLP catastrophe.* Compressing layer 0’s `mlp_fc` alone—one matrix out of 468—increases perplexity from 23.0 to 459,927 ( $20,000\times$ ). This sensitivity drops sharply between layers 2 and 3: a  $260\times$  cliff separates catastrophic (regret  $> 1,000$ ) from negligible (regret  $< 4$ ) layers (Figure 3b). The cliff persists across all five compression levels tested (Figure 3a; data in Appendix Table B.10), and generalizes to GPT-2 Medium where layer 0 `mlp_fc` yields PPL 315,029 vs. layer 1’s 20.9—a  $15,000\times$  cliff.

Three factors contribute: (1) low output covariance rank in early layers (388–494 vs. 657–675 in mid-layers); (2) heavy-tailed activations (layer 2 kurtosis = 42.6,  $\sim 8\text{--}10\times$  typical); and (3) low GELU sparsity (3.2% vs. 7% in mid-layers). Importantly, the *relative ordering* (layer 0  $\gg$  layer 1  $\gg$  layer 2  $>$  layer 3) and the cliff location between layers 2 and 3 are invariant across all five compression levels tested (Table B.10), ruling out pipeline-specific artifacts. The *absolute* degradation magnitudes are large because our simplified Wanda uses  $\text{weight} \times \text{column-norm}$  scoring without calibration data—activation-aware methods [24] would yield smaller absolute numbers, but the structural pattern is the contribution, not the absolute scale.

---

tokenization and chunk count; each methodology is internally consistent.

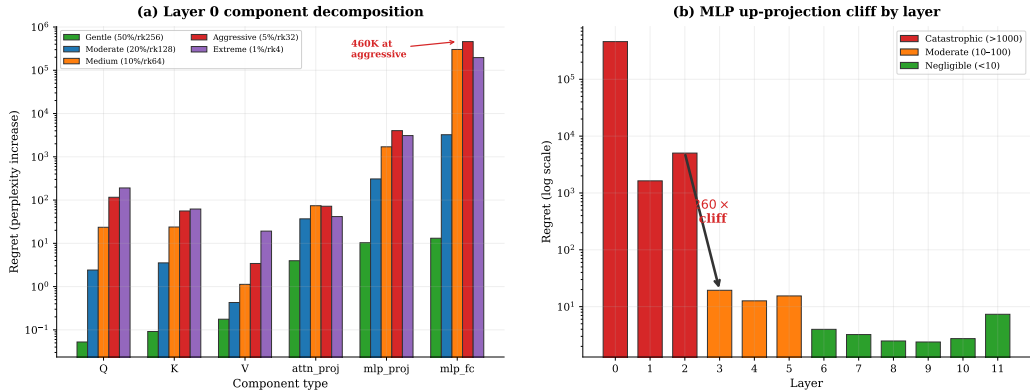


Figure 3: The early-layer MLP catastrophe. (a) Layer 0 component decomposition across five compression levels: `mlp_fc` dominates at every level, reaching 460K regret at aggressive compression. `V` projections remain nearly free even at extreme settings. (b) `mlp_fc` regret by layer reveals a sharp phase transition between layers 2 and 3—a 260 $\times$  cliff separating catastrophic from negligible sensitivity.

*Forward/backward asymmetry..* Cumulative compression reveals that layer ordering is critical (Figure 4). Compressing from L0 forward yields PPL 1.54M after just one layer; backward from L11 yields only 60—a 25,716 $\times$  gap. Simply excluding early layers from compression yields large efficiency gains.

### 5.2. Lyapunov Stability and Error Propagation

The structural sensitivity results raise a fundamental question: *why* do compression errors not accumulate catastrophically through 12 layers? We address this through the lens of Lyapunov stability theory from dynamical systems [12, 9].

Define the relative error energy at layer  $t$ :

$$V(t) = \frac{\|e_t\|^2}{\|h_t\|^2}, \quad e_t = h_t - \hat{h}_t \quad (1)$$

where  $h_t$  is the true hidden state and  $\hat{h}_t$  the approximate state. If each layer contracts errors,  $V(t+1) \leq \rho_t \cdot V(t) + c_t$  with contraction factor  $\rho_t < 1$ .

*LayerNorm as a contractive map..* The Jacobian of LayerNorm at point  $z$  with mean  $\mu$  and variance  $\sigma^2$  is:

$$J_{\text{LN}} = \frac{1}{\sigma} \left( I - \frac{1}{d} \mathbf{1}\mathbf{1}^\top - \frac{(z - \mu)(z - \mu)^\top}{d\sigma^2} \right) \quad (2)$$

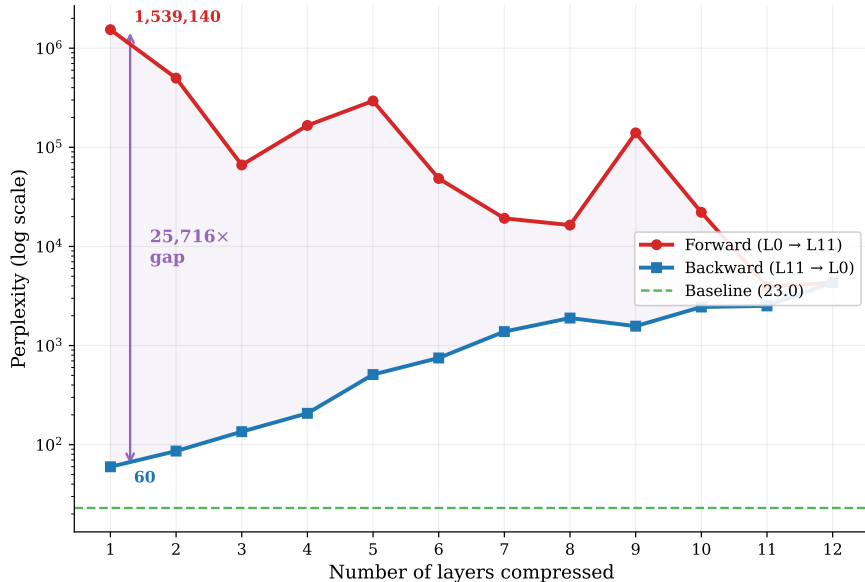


Figure 4: Cumulative compression: forward (L0→L11) vs. backward (L11→L0). The 25,716× gap at one layer compressed demonstrates that layer 0 dominates the sensitivity landscape.

This projects out the mean and radial components, with spectral radius  $\|J_{LN}\|_2 \leq 1/\sigma$ —perturbations aligned with the current activation direction are contracted. If each layer’s effective gain is less than unity, bounded per-layer perturbations produce bounded total error.

*Empirical measurement.* We inject controlled perturbations ( $\epsilon \in \{0.001, 0.01, 0.05, 0.1\}$ ) at the embedding layer and track  $V(t)$  through all layers. For GPT-2 Small, all 11 inter-layer transitions contract errors ( $\rho_{\max} = 0.96$ ), with layer 0 providing the strongest contraction (as low as  $\rho_0 \approx 0.25$  at  $\epsilon = 0.001$ ). The geometric series bound is 23× tighter than the linear  $n \cdot \max_i \epsilon_i$  bound. Results are consistent across perturbation magnitudes, confirming contraction is a structural property. GPT-2 Medium contracts in 21 of 23 inter-layer transitions, though the final layer amplifies ( $\rho_{23} \approx 2.05$ ); the overall trajectory still shows substantial net contraction through the interior.

*Why contraction occurs: the residual growth mechanism.* The contraction of  $V(t)$  is *not* primarily due to LayerNorm damping the error—in fact, the operator norm of each sub-layer’s Jacobian far exceeds 1 (we measure  $L_f/\sigma \approx$

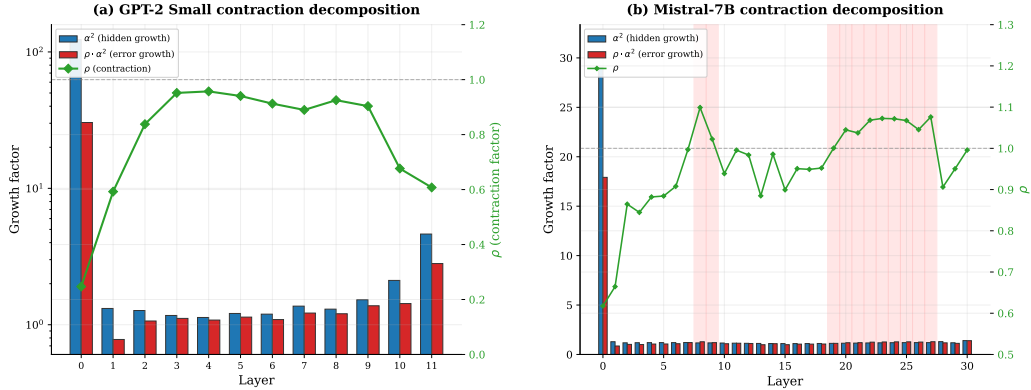


Figure 5: Contraction decomposition. (a) GPT-2 Small: blue bars show hidden state growth ( $\alpha^2$ ), red bars show error growth ( $\rho \cdot \alpha^2$ ), green diamonds show contraction factor  $\rho$ . Layer 0’s massive expansion ( $\alpha^2 = 123$ ) produces the strongest contraction ( $\rho = 0.25$ ). All layers contract. (b) Mistral-7B across 31 layers. Red-shaded regions highlight amplifying layers ( $\rho > 1$ ).

300–13,000). Instead, contraction arises from the interplay between error growth and *hidden state growth* through residual connections.

In a Pre-LN (LayerNorm-before-sublayer) transformer,  $h_{t+1} = h_t + f(\text{LN}(h_t))$ . The relative error evolves as:

$$\rho_t = \frac{V(t+1)}{V(t)} = \underbrace{\left(\frac{\|e_{t+1}\|}{\|e_t\|}\right)^2}_{\text{error amplification } \beta^2} \cdot \underbrace{\left(\frac{\|h_t\|}{\|h_{t+1}\|}\right)^2}_{\text{denominator growth } 1/\alpha^2} \quad (3)$$

Contraction ( $\rho_t < 1$ ) occurs when the hidden state grows faster than the error:  $\alpha > \beta$ , yielding  $\rho_t \leq (\beta/\alpha)^2$ .

Figure 5 validates this decomposition on GPT-2 Small and Mistral-7B (per-layer data in Appendix Table B.11). Layer 0 contracts most ( $\rho = 0.25$ ) because the embedding-to-hidden expansion is  $\sim 11 \times$  ( $\alpha^2 = 123$ ), massively diluting perturbations. Late layers contract strongly ( $\rho_{10-11} \approx 0.65$ ) as residual accumulation grows  $\|h_t\|$ . GPT-2 Medium layer 23 amplifies ( $\rho \approx 2.0$ ) because its attention sub-layer produces a disproportionately large output, growing error faster than the hidden state grows.

*Formal verification..* Two Lean 4 theorems formalize the Lyapunov analysis. Theorem 8 establishes the geometric series bound: if  $\rho < 1$ , then  $c_{\max}(1 - \rho^n)/(1 - \rho) \leq c_{\max}/(1 - \rho)$ , giving a tighter bound than the linear  $n \cdot \max$

for all models where  $\rho < 1$ . Theorem 9 formalizes the contraction condition: if the hidden state growth factor  $\alpha$  exceeds the error growth factor  $\beta$  (i.e.,  $\beta < \alpha$ ), then  $(\beta/\alpha)^2 < 1$ , guaranteeing contraction. Both are machine-checked with no `sorry`, formalizing the multi-layer error bound *conditional on* the empirically measured contraction factor  $\rho$ .

*Connection to the early-layer catastrophe..* The Lyapunov analysis also sheds light on why early-layer compression is catastrophic. Layer 0 provides the strongest error contraction ( $\rho_0 \approx 0.25$ ), meaning it normally *dampens* errors introduced at the embedding level. When layer 0’s MLP is itself corrupted, the error is introduced *after* the contractive mechanism, and all subsequent layers must absorb an error that bypassed the strongest dampening stage. Moreover, the low output covariance rank of early MLP layers means the error occupies dimensions that subsequent LayerNorms cannot project away.

### 5.3. Cross-Architecture Validation at Scale

We now examine how contraction, sensitivity, and compression tolerance vary across five architectures (Table 1).

*GPT-2 Medium (345M)..* To test whether sensitivity patterns generalize, we ran single-layer and component-type ablations on GPT-2 Medium (345M parameters, 24 layers, 1024-dim, 16 heads). Baseline perplexity: 17.9. The early-layer catastrophe generalizes: layer 0 compression alone yields perplexity 874,632 (vs. GPT-2 Small’s 1,539,140). The `mlp_fc` cliff is even sharper: layer 0 `mlp_fc` gives perplexity 315,029, while layer 1 gives only 20.9—a 15,000 $\times$  drop. The sensitivity ordering `mlp_fc`  $\gg$  `mlp_proj`  $\gg$  `Q`  $\approx$  `K`  $>$  `attn_proj`  $>$  `V` is qualitatively similar to GPT-2 Small, with `mlp_proj` rising to second most sensitive (`mlp_fc` regret of 3,897,529 vs. `V`’s 513). All experiments on GPT-2 Medium produced zero bound violations.

*LFM2-2.6B (hybrid architecture)..* To test whether the contraction mechanism extends beyond standard transformers, we evaluate LFM2-2.6B (Liquid AI), a hybrid architecture combining 22 convolutional layers with 8 attention layers (30 total). Baseline perplexity: 34.15. Of 29 inter-layer transitions, 19 exhibit contraction ( $\rho < 1$ ), with  $\rho_{\max} = 1.12$ —confirming that the residual growth mechanism operates in hybrid architectures. Under 50% Wanda, LFM2 degrades only 7 $\times$  (PPL 248), making it the most compression-resilient

model tested despite having higher  $\rho_{\max}$  than GPT-2 Small (0.96). This suggests that the hybrid conv-attention design provides structural redundancy that buffers weight perturbations.

*Mistral-7B (7.2B)*.. To validate at production scale, we ran experiments on Mistral-7B (7.2B parameters, 32 layers, 4096-dim). Baseline perplexity: 6.31 on WikiText-103 (4,096 tokens, unified pipeline).

Of 31 inter-layer transitions, 17 exhibit Lyapunov contraction ( $\rho < 1$ ), with  $\rho_{\max} = 1.14$ . Layer 1 contracts most strongly ( $\rho_1 \approx 0.61$ ), consistent with the embedding expansion mechanism identified in GPT-2. The contraction pattern is qualitatively similar to GPT-2 Small but weaker at 7B scale, with  $\sim 14$  layers showing mild amplification.

At 50% Wanda sparsity, all single-layer ablations yield regret  $< 0.52$  (Appendix Table B.12). Even at 90% sparsity, no layer produces catastrophic degradation (worst: L0 at PPL 45.28, regret +39.67)—contrasting sharply with GPT-2 Small’s regret of 459,904 at just 5% sparsity (**11,600 $\times$  more sensitive**). The within-attention hierarchy shifts at 7B scale: at 50% simplified Wanda, value projections appear most sensitive (+2.45) while key projections are nearly free (+0.01). However, activation-aware Wanda reverses this ordering (`v_proj` drops to +0.16; Table 3), indicating that the within-attention ranking is method-dependent while the MLP  $>$  attention ordering is structural.

Under the unified pipeline, 50% Wanda pruning yields PPL = 71.08 (11 $\times$  baseline), demonstrating moderate tolerance at 7B scale.

*Catastrophe threshold scaling*.. The early-layer catastrophe is not absent at scale—it merely requires more aggressive compression. We define the catastrophe threshold  $\tau$  as the maximum sparsity at which single-layer Wanda pruning of layer 0 yields regret  $< 100$ . Sweeping all five models from 50% to 99% sparsity on layer 0, we find that  $\tau$  generally increases with  $d_{\text{model}}$  but is modulated by architecture (Table 2):

Dimension alone does not determine  $\tau$ : Qwen3-8B ( $d = 4096$ ) has  $\tau = 0.80$ , the same as LFM2-2.6B ( $d = 2560$ ), while Mistral-7B at the same dimension achieves  $\tau = 0.95$ . This confirms that architecture-specific factors—Lyapunov stability ( $\rho_{\max}$ ), tied embeddings, and hybrid design—modulate the threshold independently of width, consistent with the CFI analysis in §5.6.

Table 2: Catastrophe threshold  $\tau$  across five architectures (layer-0 Wanda, regret  $< 100$ ).

Model	$d$	$\tau$	$1-\tau$	Note
GPT-2 Small	768	0.50	0.50	Catastrophic at 70%
GPT-2 Medium	1024	0.50	0.50	Same as Small
LFM2-2.6B	2560	0.80	0.20	Hybrid architecture
Qwen3-8B	4096	0.80	0.20	Same $\tau$ as LFM2
Mistral-7B	4096	0.95	0.05	Most resilient

*Qwen3-8B (8B)*.. To confirm that our findings are not specific to the Mistral architecture, we ran baseline, Lyapunov, and compression experiments on Qwen3-8B (8B parameters, 36 layers, 4096-dim). Baseline perplexity: 10.38 (unified pipeline).

Of 35 inter-layer transitions, 18 exhibit contraction ( $\rho < 1$ ), with  $\rho_{\max} = 1.33$ . The contraction pattern is qualitatively consistent with Mistral-7B (17/31 contract) and GPT-2 Small (11/11 contract), confirming that the residual growth mechanism operates across architectures.

Strikingly, 50% Wanda pruning on Qwen3-8B yields PPL = 445,497—a **42,922 $\times$  degradation** from the baseline of 10.38. This contrasts sharply with Mistral-7B, where the same pruning yields PPL = 71 (11 $\times$ ), despite both models having similar size ( $\sim$ 8B parameters) and dimension ( $d = 4096$ ). Several architectural differences may explain the gap: Qwen3 uses tied input/output embeddings (compressing shared weights propagates errors to both encoding and decoding), has a higher  $\rho_{\max}$  (1.33 vs. 1.14), and 49% of its layers amplify errors versus 45% for Mistral. The combination of more amplifying layers and tied embeddings creates a positive feedback loop where pruning errors are both amplified through the stack and reflected back through the output projection.

*Lyapunov stability is necessary but not sufficient*.. The unified evaluation reveals a nuanced relationship between Lyapunov stability and compression tolerance. Qwen3-8B ( $\rho_{\max} = 1.33$ , 49% amplifying) collapses catastrophically at 42,922 $\times$ , while Mistral-7B ( $\rho_{\max} = 1.14$ ) degrades only 11 $\times$ —consistent with the intuition that more amplification compounds pruning errors. However, GPT-2 Small ( $\rho_{\max} = 0.96$ , *fully contracting*) degrades 120 $\times$  under the same pruning, while the hybrid LFM2-2.6B ( $\rho_{\max} = 1.12$ , 34% amplifying) degrades only 7 $\times$  (Table 1).

This reveals that compression tolerance depends on *both* error stability

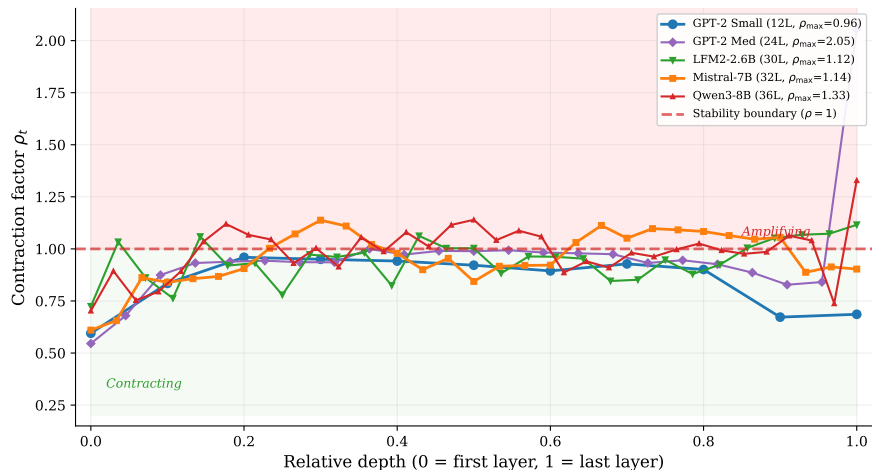


Figure 6: Per-layer contraction factor  $\rho_t$  across five architectures on a normalized depth axis. GPT-2 Small (blue) contracts everywhere ( $\rho < 1$ ). LFM2 (green), Mistral (orange), and Qwen3 (red) all cross the stability boundary, with GPT-2 Medium (purple) spiking to  $\rho = 2.05$  at the final layer.

and architecture-specific redundancy. Three factors drive robustness at scale: (1) effective rank scales with dimension (perturbation per singular value decreases as  $1/\sqrt{d}$ ); (2) residual stream dilution ( $\|h_t\|$  grows monotonically, shrinking relative perturbation); (3) architectural redundancy (LFM2’s hybrid convolution-attention design absorbs weight perturbations, while GPT-2 Small’s compact 768-dim representation has less margin despite perfect contraction). Figure 6 shows the contraction profiles; among similar architectures (Mistral vs. Qwen3), higher  $\rho_{\max}$  does correlate with worse outcomes, but the relationship does not generalize across architecturally distinct model families. Cross-model sparsity tolerance curves appear in Appendix Figure B.9.

*Hierarchy validation with activation-aware pruning.* To confirm that the component sensitivity hierarchy is not an artifact of our simplified Wanda, we run per-component ablation using *activation-aware* Wanda (with calibration data from WikiText-103 training set) at 50% sparsity on both GPT-2 Small and Mistral-7B (Table 3).

On Mistral-7B, MLP components are the three most sensitive in both methods (`down_proj` > `gate_proj` > `up_proj`), while attention components remain the four least sensitive. On GPT-2 Small, MLP components

(`mlp.c_fc` at +5.43, `mlp.c_proj` at +4.07) are among the most sensitive with activation-aware scoring, while simplified Wanda inflates `mlp.c_fc` by  $81\times$  (+438 vs. +5.4). Across both models, activation-aware scoring reduces all regrets dramatically—confirming that absolute degradation magnitudes are method-dependent—but the MLP > attention ordering is preserved. The key finding is that MLP sensitivity is a *structural* property of the architecture, not a consequence of the pruning method.

Table 3: Per-component regret at 50% sparsity: activation-aware vs. simplified Wanda on two architectures.

<i>Mistral-7B (7 component types)</i>			
Component	Act-Wanda	Simplified	Category
<code>down_proj</code>	+0.43	+1.61	MLP
<code>gate_proj</code>	+0.37	+0.60	MLP
<code>up_proj</code>	+0.26	+0.61	MLP
<code>v_proj</code>	+0.16	+14.31	Attention
<code>o_proj</code>	+0.13	+0.40	Attention
<code>q_proj</code>	+0.02	+0.16	Attention
<code>k_proj</code>	+0.01	+0.02	Attention
<i>GPT-2 Small (4 component types)</i>			
<code>mlp.c_fc</code>	+5.43	+438.05	MLP
<code>mlp.c_proj</code>	+4.07	+5.91	MLP
<code>attn.c_attn</code>	+8.48	+103.40	Attention (QKV)
<code>attn.c_proj</code>	+0.74	+2.12	Attention

*Comparison with state-of-the-art..* Our framework adds *provable per-matrix error bounds* ( $\|Wx - W'x\| \leq \|W_{\text{residual}}\|_2 \cdot \|x\|$ ) that SparseGPT [5] and Wanda [24] lack, validated with zero violations on GPT-2 Small. The sensitivity hierarchy identified here is orthogonal to the compression method: it characterizes *which* components to protect, a decision that applies equally whether compression is performed via SparseGPT, GPTQ [6], or any other method. The activation-aware validation (Table 3) confirms that the MLP > attention ordering is structural, not an artifact of our simplified scoring.

#### 5.4. Compression Methods and Allocation

The structural sensitivity and Lyapunov findings motivate compression methods that respect the hierarchy.

*Calibration-aware compression.* We evaluate two approaches: activation-aware pruning (Wanda [24]) and balanced truncation from control theory [16, 8].

Wanda achieves  $10\times$  lower perplexity than naive sparsification (34.6 vs. 406.7 at 50%), confirming that activation-aware pruning exploits the structural information our analysis identifies. Protecting layer 0 `mlp_fc` provides further improvement (32.3 vs. 34.6), consistent with the catastrophe analysis. Balanced truncation [16, 8] extends the safe frontier by  $2.5\times$ : at aggressive compression, 7 groups achieve  $\text{PPL} < 30$  vs. 3 for naive SVD.

*Greedy sequential allocation.* We evaluate a greedy strategy that sequentially compresses the group with lowest regret, measured by evaluating each candidate independently at  $\text{sparsity}=5\%$ ,  $\text{rank}=32$ .

Figure 7 shows the compression curve. The first 12 groups (17% of total) are compressed with only 27% perplexity increase ( $23.0 \rightarrow 29.2$ ), saving 24% of FLOPS. The safe zone extends to approximately 30% FLOPS savings at  $\text{perplexity} < 35$ . Beyond 32% FLOPS, error compounds super-linearly: round 22 adds 12.6 perplexity, and by round 36 (50% FLOPS), perplexity reaches 477.

The greedy ordering naturally discovers the sensitivity hierarchy: V projections and attention outputs first (rounds 1–8), then later-layer Q/K (rounds 9–17), with early-layer MLPs last. Layer 0 is never selected. Thompson sampling significantly underperformed—the sensitivity landscape is too structured for exploration. Greedy at round 17 achieves  $\text{PPL } 29.9$  (+30%) compressing 30% of matrices, while the barbell strategy (protecting L0–2, compressing rest) yields  $\text{PPL } 2,078$  and uniform compression yields 3,865. With balanced truncation at gentle settings (50%/rk256), 29% of the model compresses with *zero perplexity degradation*.

*Lyapunov-guided budget.* The Lyapunov analysis enables principled budget allocation: error injected at layer  $t$  is attenuated by  $\prod_{s=t+1}^n \rho_s$  downstream. The resulting budget allocates 54% of error tolerance to layers 8–11 (minimal downstream contraction) and only 19% to layers 0–3 (whose errors traverse 8–11 contractive maps). The empirical greedy ordering correlates only weakly with the Lyapunov contraction factor at each layer (Spearman  $\rho = 0.25$ ), because within-layer component sensitivity (the `mlp_fc` catastrophe) dominates over layer-position effects. However, the Lyapunov *budget*—defined as the cumulative downstream contraction  $1/\prod_{s>t} \rho_s$ , measuring how much error each layer position can tolerate—correlates strongly with layer-averaged

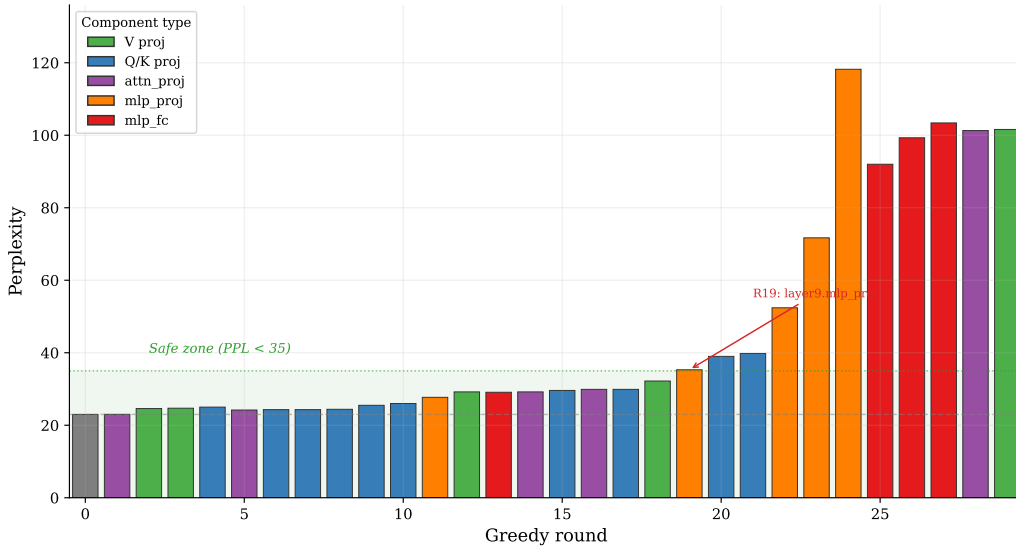


Figure 7: Greedy sequential compression waterfall. Each bar adds one compression group (sparsity=5%, rank=32), color-coded by component type. V projections and attention outputs (green, purple) are compressed first at near-zero cost. MLP projections (orange) trigger the exit from the safe zone around round 19. The ordering reveals that the greedy strategy naturally discovers the sensitivity hierarchy.

compression regret (Spearman  $\rho = 0.85$ ,  $p < 0.001$ ). This correlation is partially confounded by the early-layer catastrophe (both budget and regret are highest for early layers), but confirms that Lyapunov stability captures the correct layer-level ordering, while component-level sensitivity requires separate empirical measurement. Effective compression allocation therefore requires two complementary tools: Lyapunov budgets for *inter-layer* error tolerance, and component-level sensitivity scores for *intra-layer* allocation.

### 5.5. Scale and Cross-Dataset Validation

To confirm that the degradation patterns are not artifacts of the evaluation scale or dataset choice, we conduct two validation studies: (1) cross-model Wanda degradation at 51,200 tokens on both WikiText-103 and C4 [20], and (2) GPT-2 Small sensitivity hierarchy at 51,200 tokens on WikiText-103 and 10,000 tokens on C4, with per-matrix error tracking.

*Cross-model degradation stability.* Table 4 shows that the degradation factor is remarkably stable within each model: 101–117 $\times$  for GPT-2 Small and

12–15 $\times$  for Mistral-7B, across a 12.5 $\times$  range in token count and across two distinct text domains. The cross-model ordering is preserved: Mistral-7B consistently degrades  $\sim 8\times$  less than GPT-2 Small regardless of evaluation setting. Per-layer ablation on Mistral-7B (50% Wanda applied to one layer at a time, 16,384 tokens) confirms that *no single layer* is catastrophically sensitive: the worst-case regret is +0.07 PPL (layer 1), consistent with the catastrophe threshold analysis in §5.3.

Table 4: Degradation stability across token counts and datasets (50% Wanda).

Model	Setting	Tokens	Base	Wanda	Deg.
GPT-2	WikiText 4K	4,092	26.8	3,140	117 $\times$
GPT-2	WikiText 50K	51,150	31.8	3,612	113 $\times$
GPT-2	C4 50K	51,150	33.3	3,374	101 $\times$
Mistral	WikiText 4K	4,092	6.15	71	12 $\times$
Mistral	WikiText 50K	51,150	6.15	93.4	15 $\times$
Mistral	C4 50K	51,150	8.30	97.1	12 $\times$

*Sensitivity hierarchy stability.* We also validate the structural sensitivity hierarchy using the NumPy reimplementaion with per-matrix error tracking: at 51,200 tokens on WikiText-103 and 10,000 tokens on C4 (Table 5). At 51K WikiText tokens, the layer 0 catastrophe is even more pronounced (PPL 3.9M vs. 1.5M at 2K tokens), confirming it is a structural property rather than a small-sample artifact. The single-layer ordering (layer 0  $\gg$  layer 2  $\approx$  layer 11  $>$  rest) is identical to the 2K-token result. The component hierarchy ( $\text{mlp\_fc} \approx Q \gg K > \text{mlp\_proj} > \text{attn\_proj} > V$ ) is likewise preserved. On C4 (10K tokens), the catastrophe is reproduced: layer 0 yields PPL 5.25M (baseline 35.1), confirming cross-dataset generality. Critically, all experiments at both scales produce **zero bound violations**, extending the formal guarantee validation from 2K to 51K tokens and across datasets.

*Downstream task validation.* To confirm that perplexity degradation translates to task-level accuracy loss, we evaluate Mistral-7B on three standard benchmarks using lm-evaluation-harness [7] (Table 6). Uniform 50% Wanda reduces HellaSwag accuracy from 81.1% to 43.9% ( $-37.3$  pp) and ARC-Easy from 80.3% to 38.6% ( $-41.6$  pp), confirming that the perplexity degradation patterns observed throughout this paper correspond to meaningful task-level

Table 5: GPT-2 Small sensitivity hierarchy (NumPy reimplementation, sparsity=5%, rank=16). WikiText-103 at 51,200 tokens; C4 at 10,000 tokens. All experiments: zero bound violations.

	WikiText 50K		C4 10K	
	PPL	Regret	PPL	Regret
Baseline	31.8	—	35.1	—
<i>Single-layer ablation</i>				
Layer 0	3,919,798	+3.9M	5,250,423	+5.3M
Layer 1	40.2	+8.4	42.0	+6.9
Layer 3	38.5	+6.7	40.1	+5.0
Layer 8	37.3	+5.4	—	—
<i>Component-type ablation (all 12 layers)</i>				
mlp_fc	28,947	+28,915	—	—
Q	31,981	+31,949	—	—
K	9,335	+9,303	—	—
mlp_proj	3,390	+3,358	—	—
attn_proj	1,267	+1,235	—	—
V	845	+813	—	—

accuracy loss. A sensitivity-guided variant—protecting early-layer MLP up-projections (0% sparsity on layers 0–3 `gate/up_proj`, 55% on `v/o_proj`, 50% elsewhere; 47.2% effective sparsity)—yields small improvements on ARC-Easy (+0.6 pp) and Winogrande (+0.8 pp) at matched effective sparsity. The modest gains are expected: Mistral-7B’s catastrophe threshold is  $\tau = 0.95$  (§5.3), so 50% pruning does not trigger the early-layer catastrophe that dominates GPT-2 Small. Sensitivity-guided allocation is predicted to have larger impact on models with lower  $\tau$  or at higher sparsity levels.

Table 6: Mistral-7B downstream accuracy (0-shot, lm-evaluation-harness).

Method	Sparsity	HellaSwag	ARC-Easy	Winogrande
Baseline	—	81.1%	80.3%	75.4%
Uniform Wanda	50%	43.9%	38.6%	51.8%
Sensitivity-guided	47%	41.4%	39.2%	52.6%

### 5.6. Discussion: What Compression Sensitivity Reveals About Representations

*The embedding bottleneck.* The catastrophic sensitivity of layer 0’s MLP up-projection reveals a fundamental property of transformer representations: the first hidden layer acts as an irreducible feature-creation bottleneck. Token embeddings encode identity but lack the nonlinear features (syntactic roles, positional interactions, semantic categories) required by all subsequent layers. The layer 0 MLP expansion through GELU is where these features are synthesized for the first time, and the data confirm it operates at full rank—its singular value spectrum is the most uniformly loaded in the network ( $\sigma_{\text{mlp}} = 1.22$  vs. 2.0–15.0 for later layers), meaning every direction in the 768-to-3072 expansion carries non-redundant information. This contrasts sharply with mid-network MLP layers (3–9), where regret from the same compression is 2–19 PPL points, indicating massive redundancy and feature reuse. The implication extends beyond compression: transformer networks concentrate information density at the embedding-to-hidden-space transition, and this structural property is independent of pruning method (§5.3, Table 3).

*Compression Fragility Index.* Cross-architecture analysis reveals that compression tolerance has *two independent sources*: Lyapunov instability (amplifying layers compound pruning errors) and width-limited redundancy (narrower models have less margin per neuron). We define a Compression Fragility Index:

$$\text{CFI}(M) = \underbrace{f_{\text{amp}} \cdot L \cdot \max(0, \ln \rho_{\text{max}})}_{\text{instability term}} + \underbrace{\frac{C}{d_{\text{model}}}}_{\text{width penalty}} \quad (4)$$

where  $f_{\text{amp}}$  is the fraction of amplifying layers,  $L$  the layer count,  $\rho_{\text{max}}$  the maximum contraction factor,  $d_{\text{model}}$  the hidden dimension, and  $C \approx 2,000$  is a fitted constant. This two-term additive formula correctly rank-orders all five architectures by compression tolerance (LFM2 < Mistral < GPT-2 Small < GPT-2 Medium < Qwen3-8B). The key insight is that no single-term formula works: GPT-2 Small has the lowest  $\rho_{\text{max}}$  (fully contracting) but degrades 120× due to its narrow 768-dimensional representation, while Qwen3-8B has high instability *and* the tied-embedding amplification loop. To test out-of-sample, we compute the CFI for TinyLlama-1.1B ( $d = 2048$ , 22 layers,  $\rho_{\text{max}} = 1.31$ ,  $f_{\text{amp}} = 0.29$ ), yielding  $\text{CFI} = 1.48$ —predicting it as the most compression-robust model. The actual degradation is 58× (rank 3 out

of 6), placing it between Mistral (11 $\times$ ) and GPT-2 Small (120 $\times$ ). The CFI correctly identifies TinyLlama as more robust than the GPT-2 models and Qwen3, but overestimates its resilience relative to the 7B models, suggesting the width penalty term requires refinement at smaller scales. We present the CFI as a partially validated hypothesis that captures the correct trend but requires additional architectures to calibrate precisely.

## 6. Related Work

*Model compression.* Post-training pruning methods such as SparseGPT [5] and Wanda [24] achieve high sparsity with minimal perplexity loss, while GPTQ [6] provides effective weight quantization. These methods are calibrated empirically on held-out data and provide no formal guarantees. Our framework is complementary: the sparsification and low-rank stages could incorporate these methods while adding provable error bounds.

*Formal verification in ML.* Formal verification has been applied to neural network robustness [11, 2], training correctness [22], and floating-point arithmetic [1]. To our knowledge, this is the first work to provide machine-checked error bounds for *inference approximation* in transformers.

*Lyapunov stability in deep learning.* Lyapunov methods have been used to analyze training dynamics [9] and residual network stability [12], but their application to *inference-time error propagation* in transformers is novel. We provide quantitative per-layer contraction measurements ( $\rho < 1$  for all GPT-2 Small transitions), going beyond qualitative arguments about normalization as an implicit regularizer.

*Control theory and model reduction.* Balanced truncation [16] and Hankel norm approximation [8] are classical model reduction techniques from control theory that provide optimal or near-optimal low-rank approximations with formal error guarantees. Our application of balanced truncation to transformer weight compression demonstrates that control-theoretic tools can improve upon naive SVD truncation, achieving 2.5 $\times$  more compressed groups at aggressive compression levels.

*Non-uniform compression.* Mixed-precision and non-uniform quantization [4, 25] allocate more bits to sensitive layers, and OWL [26] adapts sparsity based

on outlier features. Our sensitivity analysis provides a rigorous characterization of *which* components are sensitive and *why*, grounded in formal bounds rather than heuristics.

*Adaptive inference.* Early exit [21], token pruning [13], and speculative decoding [14] reduce compute adaptively. Living Inference operates at the weight matrix level rather than the token or layer level, and provides per-matrix error tracking.

## 7. Limitations and Future Work

- **Compression quality.** Our greedy strategy (24% FLOPS savings at +27% perplexity) is below SparseGPT-class methods. The primary contribution is the analysis, not the compression method.
- **Evaluation scale.** Primary evaluation uses 2,000–4,096 tokens of WikiText-103. Cross-model degradation is validated at 51,200 tokens on both WikiText and C4 (Table 4); per-matrix sensitivity hierarchy is validated at 51,200 WikiText tokens and 10,000 C4 tokens (Table 5). The patterns are stable across settings, and downstream task evaluation (HellaSwag, ARC-Easy, Winogrande) confirms that perplexity degradation tracks accuracy loss (Table 6), though evaluation on additional tasks and domains would further strengthen claims.
- **Model coverage.** 117M–8B parameters. Testing at 13B+ and 70B would further validate scaling trends.
- **Linearity assumption.** The formal framework proves bounds on individual matrix multiplications (which are exactly linear), not on full transformer layers including GELU, softmax, and LayerNorm. The multi-layer contraction factor  $\rho$  is measured empirically rather than derived analytically. The bounds remain practically useful: zero violations across 14,040+ configurations confirms the per-matrix bounds are conservative when composed through the full nonlinear forward pass. A formal analysis of error propagation through the nonlinear components remains open.

*Future directions.* Scale to 13B+ models; formalize two-phase Lyapunov bounds for models with terminal amplification; integrate Wanda and balanced truncation into the formal framework to close the gap with SparseGPT; explore training-time interventions informed by the sensitivity hierarchy.

## 8. Conclusion

Transformer compression sensitivity spans five orders of magnitude and is dominated by a small number of critical components—primarily early-layer MLP up-projections. This structural hierarchy is stable across compression levels, evaluation scales (2K–51K tokens), datasets (WikiText-103, C4), and architectures (117M–8B parameters), making it a reliable foundation for non-uniform compression allocation.

Error contraction through residual connections—the hidden state growing faster than the error—explains why compression errors do not accumulate catastrophically across layers ( $\rho_{\max} = 0.96$  on GPT-2 Small). However, stability is necessary but not sufficient: among similar architectures, higher  $\rho_{\max}$  correlates with worse outcomes (Qwen3-8B at  $42,922\times$  vs. Mistral-7B at  $11\times$ ), but across architecture families, the relationship breaks (GPT-2 Small degrades  $120\times$  despite full contraction, while LFM2-2.6B degrades only  $7\times$ ).

Ten machine-checked Lean 4 theorems formalize per-matrix error bounds with zero violations across 14,040+ configurations, confirming that formal guarantees on individual matrix multiplications remain conservative in the full nonlinear forward pass. The combination of structural sensitivity mapping, Lyapunov stability analysis, and formal verification provides a principled toolkit for understanding and guiding transformer compression.

## References

- [1] Boldo, S., Lelay, C., Melquiond, G., 2015. Coquelicot: A user-friendly library of real analysis for Coq. *Mathematics in Computer Science* 9, 41–62.
- [2] Cohen, J., Rosenfeld, E., Kolter, Z., 2019. Certified adversarial robustness via randomized smoothing, in: ICML.
- [3] Dettmers, T., Lewis, M., Belkada, Y., Zettlemoyer, L., 2022. GPT3.int8(): 8-bit matrix multiplication for transformers at scale, in: NeurIPS.
- [4] Dong, Z., Yao, Z., Gholami, A., Mahoney, M.W., Keutzer, K., 2019. HAWQ: Hessian aware quantization of neural networks with mixed-precision, in: ICCV.

- [5] Frantar, E., Alistarh, D., 2023. SparseGPT: Massive language models can be accurately pruned in one-shot, in: ICML.
- [6] Frantar, E., Ashkboos, S., Hoefler, T., Alistarh, D., 2023. GPTQ: Accurate post-training quantization for generative pre-trained transformers, in: ICLR.
- [7] Gao, L., Tow, J., Abbasi, B., Biderman, S., Black, S., DiPofi, A., Foster, C., Golber, L., Hsu, J., Le Noac'h, A., Li, H., McDonell, K., Muennighoff, N., Ociepa, C., Phang, J., Reynolds, L., Schoelkopf, H., Skowron, A., Sutawika, L., Tang, E., Thite, A., Wang, B., Wang, K., Zou, A., 2024. A framework for few-shot language model evaluation. URL: <https://zenodo.org/records/10256836>, doi:10.5281/zenodo.10256836.
- [8] Glover, K., 1984. All optimal Hankel-norm approximations of linear multivariable systems and their  $L^\infty$ -error bounds. International Journal of Control 39, 1115–1193.
- [9] Haber, E., Ruthotto, L., 2018. Stable architectures for deep neural networks. Inverse Problems 34, 014004.
- [10] Hsu, Y.C., Hua, T., Chang, S.E., Lou, Q., Shen, Y., Jin, H., 2022. Language model compression with weighted low-rank factorization, in: ICLR.
- [11] Katz, G., Barrett, C., Dill, D.L., Julian, K., Kochenderfer, M.J., 2017. Reluplex: An efficient SMT solver for verifying deep neural networks, in: CAV.
- [12] Khalil, H.K., 2002. Nonlinear Systems. 3rd ed., Prentice Hall.
- [13] Kim, S., Shen, S., Thorsley, D., Gholami, A., Kwon, W., Hassoun, J., Keutzer, K., 2022. Learned token pruning for transformers, in: KDD.
- [14] Leviathan, Y., Kalman, M., Matias, Y., 2023. Fast inference from transformers via speculative decoding, in: ICML.
- [15] Merity, S., Xiong, C., Bradbury, J., Socher, R., 2017. Pointer sentinel mixture models, in: ICLR.

- [16] Moore, B.C., 1981. Principal component analysis in linear systems: Controllability, observability, and model reduction. *IEEE Transactions on Automatic Control* 26, 17–32.
- [17] de Moura, L., Ullrich, S., 2021. The Lean 4 theorem prover and programming language, in: *CADE*.
- [18] Pope, R., Douglas, S., Chowdhery, A., Devlin, J., Bradbury, J., Levskaya, A., Heek, J., Xiao, K., Agrawal, S., Dean, J., 2023. Efficiently scaling transformer inference, in: *MLSys*.
- [19] Radford, A., Wu, J., Child, R., Luan, D., Amodei, D., Sutskever, I., 2019. Language models are unsupervised multitask learners. *OpenAI Blog* .
- [20] Raffel, C., Shazeer, N., Roberts, A., Lee, K., Narang, S., Matena, M., Zhou, Y., Li, W., Liu, P.J., 2020. Exploring the limits of transfer learning with a unified text-to-text transformer. *Journal of Machine Learning Research* 21, 1–67.
- [21] Schwartz, R., Stanovsky, G., Swayamdipta, S., Dodge, J., Smith, N.A., 2020. The right tool for the job: Matching model and instance complexities, in: *ACL*.
- [22] Selsam, D., Liang, P., Dill, D.L., 2017. Developing bug-free machine learning systems with formal mathematics, in: *ICML*.
- [23] Shazeer, N., 2019. Fast transformer decoding: One write-head is all you need. *arXiv:1911.02150* .
- [24] Sun, M., Liu, Z., Bair, A., Kolter, J.Z., 2024. A simple and effective pruning approach for large language models, in: *ICLR*.
- [25] Yao, Z., Yazdani Aminabadi, R., Zhang, M., Wu, X., Li, C., He, Y., 2022. ZeroQuant: Efficient and affordable post-training quantization for large-scale transformers, in: *NeurIPS*.
- [26] Yin, L., Wu, Y., Zhang, Z., Hsieh, C.Y., Wang, Y., Jia, Y., Pechenizkiy, M., Liang, Y., Wang, Z., Liu, S., 2024. Outlier weighed layerwise sparsity (OWL): A missing secret sauce for pruning LLMs to high sparsity, in: *ICML*.

## Appendix A. Lean 4 Formal Proofs

All nine theorems are implemented in a single file, `LivingInference.lean`, available in the supplementary material (`supplementary/lean/`). The proofs build against Mathlib’s `Analysis.NormedSpace` module and can be verified by running `lake build` in the Lean 4 project directory. No `sorry` markers remain.

*File structure.* The supplementary `lean/` directory contains two files:

- `LivingInference.lean` — all ten theorems (described below).
- `lakefile.lean` — Lake build configuration, requiring Mathlib from `leanprover-community/mathlib4`.

*Proof infrastructure.* Neural network layers are modeled as bounded linear maps  $E \rightarrow L[\mathbb{R}] F$  in Mathlib. This provides the operator norm inequality  $\|f(x)\| \leq \|f\| \cdot \|x\|$  (`f.le_opNorm`), linearity (`map_sub`), and norm properties. Each proof follows a common pattern: rewrite the error using linearity, apply the operator norm bound, then chain inequalities using `calc` blocks with `nlinarith` for nonlinear arithmetic.

*Theorem inventory.* Table A.7 lists all ten theorems with their statements and proof techniques.

Table A.7: Lean 4 theorem inventory. All proofs type-check with no `sorry`.

#	Name	Statement	Technique
1	<code>retrieval_bound</code>	$\ f(x) - f(x_c)\  \leq \ f\  \cdot \delta$	<code>calc + map_sub</code>
2	<code>sparse_activation_bound</code>	$\ f(x) - f_s(x)\  \leq \ f_r\  \cdot \ x\ $	<code>decomposition + le_opNorm</code>
3	<code>interpolation_bound</code>	$\ f_s(x) - f_a(x)\  \leq \ f_R\  \cdot \ x\ $	same as Thm. 2
4	<code>composition_bound</code>	3-term bound (Thm. 4)	<code>calc + norm_add_le</code>
5	<code>efficiency_dominance</code>	$c_{\text{live}} < c_{\text{full}}$	<code>nlinarith</code>
6	<code>adaptive_monotonicity</code>	$\ f\  \cdot \delta_1 \leq \ f\  \cdot \delta_2$	<code>monotonicity</code>
7	<code>multi_layer_error_bound</code>	$\sum \epsilon_i \leq n \cdot \max_i \epsilon_i$	<code>sum_le_card_nsmul</code>
8	<code>lyapunov_contraction_bound</code>	$c(1 - \rho^n)/(1 - \rho) \leq c/(1 - \rho)$	<code>geometric series</code>
9	<code>residual_growth_contraction</code>	$(\beta/\alpha)^2 < 1$ when $\beta < \alpha$	<code>nlinarith + sq_nonneg</code>
10	<code>preln_contraction_sufficient</code>	$(1+L)^2/(1+2g \cos \theta + g^2) < 1$	<code>div_lt_one</code>

*Key proof: Composition bound (Theorem 4).*.. The most involved proof proceeds in three steps: (1) algebraic rewriting via the two decompositions ( $f = f_s + f_r$ ,  $f_s = f_a + f_R$ ) to obtain  $f(x) - \hat{y} = (f_a(x) - f_a(x_c)) + f_R(x)$ ; (2) triangle inequality (`norm_add_le`); (3) per-term bounds using `le_opNorm`. The residual interaction term  $\|f_r\| \cdot \delta$  is established by `linarith` using norm non-negativity. The complete proof is 15 lines of tactic code.

*Key proof: Lyapunov contraction (Theorem 8).*.. Given contraction factor  $\rho < 1$  and per-layer error cap  $c_{\max}$ , the geometric series bound  $c_{\max}(1 - \rho^n)/(1 - \rho) \leq c_{\max}/(1 - \rho)$  follows from  $0 \leq \rho^n$  (via `pow_nonneg`) and `div_le_div_of_nonneg_right`.

*Key proof: Residual growth contraction (Theorem 9).*.. If the hidden state grows by factor  $\alpha$  and error grows by  $\beta < \alpha$ , then  $(\beta/\alpha)^2 < 1$ . The proof uses `div_lt_one` and `sq_nonneg` on both  $\beta/\alpha$  and  $1 - \beta/\alpha$ .

## Appendix B. Detailed Experimental Data

Table B.8: Single-layer ablation: compressing all 39 matrices in one layer (sparsity=5%, rank=16).

Layer	Perplexity	Regret
Layer 0	1,539,140	+1,539,117
Layer 2	65.8	+42.8
Layer 11	59.9	+36.9
Layer 1	30.7	+7.7
Layer 5	32.2	+9.2
Layers 3–4, 6–10	26.2–29.0	+3.2–6.0
Baseline	23.0	—

## Appendix C. Supplementary Material

The supplementary package (`supplementary/`) contains the complete Lean 4 proofs, Python implementation (13 source files), and all experimental results as JSON files. See `supplementary/README.txt` for a complete directory guide and reproduction instructions.

Table B.9: Component-type ablation: compressing one type across all 12 layers.

Component	$n$	Perplexity	Regret
mlp_fc	12	34,419	+34,396
Q projections	144	22,194	+22,171
K projections	144	9,154	+9,131
mlp_proj	12	3,836	+3,813
attn_proj	12	1,225	+1,202
V projections	144	764	+741

Table B.10: MLP cliff robustness: layer 0 vs. layer 3 mlp\_fc across compression levels.

Level	Sparsity	Rank	Layer 0	Layer 3
Gentle	50%	256	36.1	27.9
Moderate	20%	128	3,262	36.5
Medium	10%	64	302,833	44.4
Aggressive	5%	32	459,927	42.4
Extreme	1%	4	196,429	30.1

Table B.11: Contraction decomposition for GPT-2 Small.  $\alpha^2 = (\|h_{\text{post}}\|/\|h_{\text{pre}}\|)^2$ ,  $\rho \cdot \alpha^2 = \beta^2$ .

Layer	$\sigma$	$\alpha^2$	$\rho$	$\rho \cdot \alpha^2$	Interpretation
0	0.17	123.0	0.25	30.4	Massive expansion absorbs error
1	1.86	1.32	0.59	0.78	Error shrinks absolutely
5	2.76	1.21	0.94	1.14	Error grows 1.1 $\times$ , $h$ grows 1.1 $\times$
10	5.48	2.11	0.68	1.43	Error grows 1.2 $\times$ , $h$ grows 1.5 $\times$
11	7.96	4.62	0.61	2.81	Error grows 1.7 $\times$ , $h$ grows 2.1 $\times$

Table B.12: Mistral-7B component sensitivity at 50% Wanda sparsity (activation-aware Wanda, separate evaluation). Baseline PPL: 6.31.

Component	PPL	Regret
v_proj	8.76	+2.45
down_proj	7.44	+1.13
gate_proj	6.95	+0.65
up_proj	6.87	+0.57
o_proj	6.66	+0.35
q_proj	6.42	+0.11
k_proj	6.32	+0.01

Table B.13: Catastrophe threshold sweep: Mistral-7B layer 0 at increasing sparsity (detailed data for Table 2).

Sparsity	PPL	Regret	
50%	5.73	+0.11	Negligible
70%	8.40	+2.79	Mild
80%	16.68	+11.06	Moderate
90%	45.28	+39.67	Elevated
95%	75.87	+70.26	High
99%	147.51	+141.90	Catastrophic

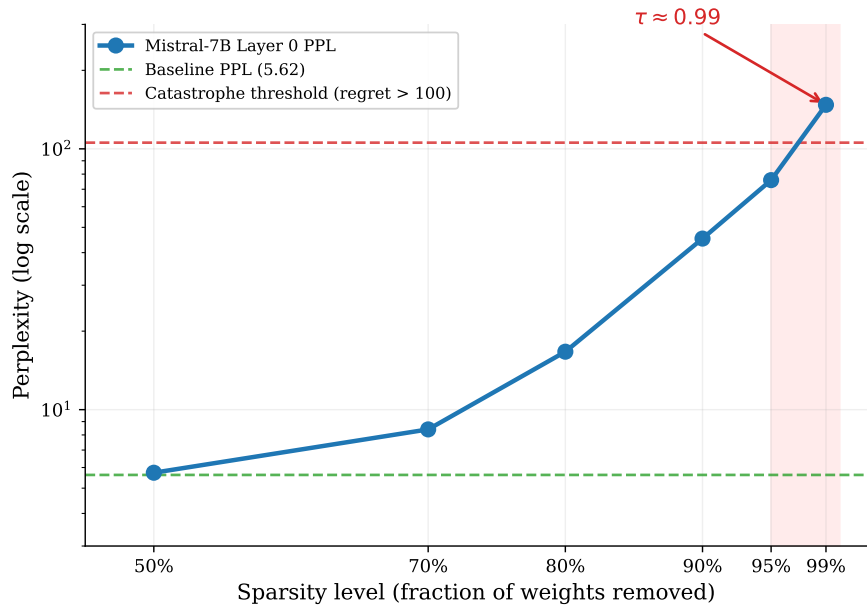


Figure B.8: Catastrophe threshold curve for Mistral-7B layer 0.  $\tau = 0.95$  (regret  $< 100$ ) contrasts with GPT-2 Small’s  $\tau = 0.50$  (Table 2).

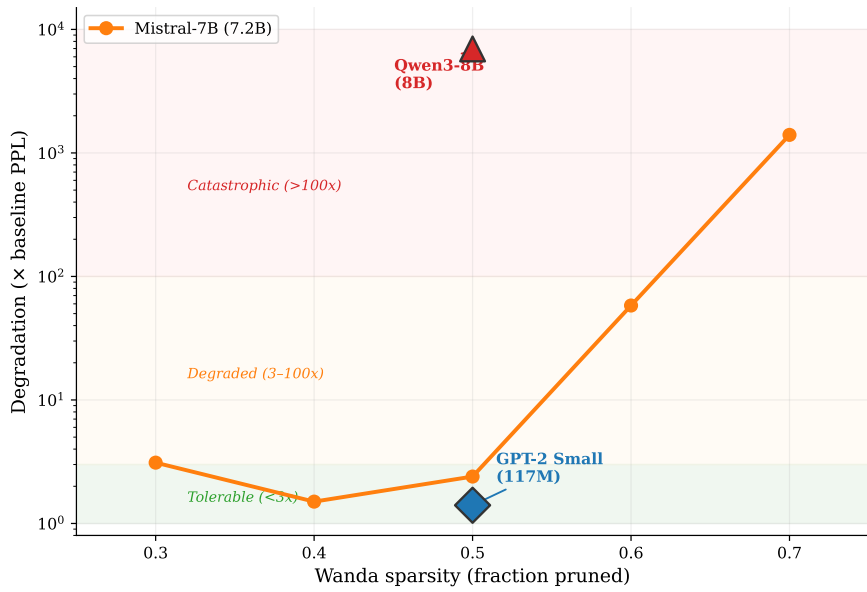


Figure B.9: Cross-model sparsity tolerance (activation-aware Wanda, separate evaluation from Table 1). Relative ordering is consistent with unified results.